Research Article | Vol. 24, No. 23 | 14 Nov 2016 | OPTICS EXPRESS 26024
Optics EXPRESS

Exploiting concave-convex linear resonators to design end-pumped solid-state lasers with flexible cavity lengths: application for exploring the self-mode-locked operation

P. H. TUAN,[1] C. C. CHANG,[1] C. Y. LEE,[1] C. Y. CHO,[1] H. C. LIANG,[2] AND Y. F. CHEN[1,*]

[1]*Department of Electrophysics, National Chiao Tung University, 1001, Ta-Hsueh Rd., Hsinchu 30010, Taiwan*
[2]*Institute of Optoelectronic Science, National Taiwan Ocean University, 2 Pei-Ning Rd., Keelung 20224, Taiwan*
[*]*yfchen@cc.nctu.edu.tw*

Abstract: The characteristics of a convex-concave linear resonator under the thermal lensing effect are theoretically analyzed to find an analytical model for designing end-pumped solid-state lasers with flexible cavity lengths. By exploiting the design model, the power scaling for continuous-wave operation under strong thermal lensing can be easily achieved in the proposed resonator with different cavity lengths. Furthermore, the proposed resonator is applied to explore the exclusive influence of cavity length on the self-mode-locked (SML) operation. It is discovered that the lasing longitudinal modes will split into multiple groups in optical spectrum to lead to a multi-pulse mode-locked temporal state when the cavity length increases. Finally, a theoretical model is derived to reconstruct the experimental results of SML operation to deduce a simple relationship between the group number of lasing modes and the cavity length.

OCIS codes: (140.3410) Laser resonators; (140.3480) Lasers, diode-pumped; (140.4050) Mode-locked lasers.

References and links

1. T. Y. Fan and R. L. Byer, "Diode laser-pumped solid-state lasers," IEEE J. Quantum Electron. **24**(6), 895–912 (1988).
2. W. Koechner, "Thermal lensing in a Nd:YAG laser rod," Appl. Opt. **9**(11), 2548–2553 (1970).
3. M. E. Innocenzi, H. T. Yura, C. L. Fincher, and R. A. Fields, "Thermal modeling of continuous-wave end-pumped solid-state lasers," Appl. Phys. Lett. **56**(19), 1831–1833 (1990).
4. S. C. Tidwell, J. F. Seamans, M. S. Bowers, and A. K. Cousins, "Scaling CW diode-end-pumped Nd:YAG lasers to high average powers," IEEE J. Quantum Electron. **28**(4), 997–1009 (1992).
5. Y. F. Chen, C. F. Kao, T. M. Huang, C. L. Wang, and S. C. Wang, "Influence of thermal effect on output power optimization in fiber-coupled laser-diode end-pumped lasers," IEEE J. Sel. Top. Quantum Electron. **3**(1), 29–34 (1997).
6. W. A. Clarkson, "Thermal effects and their mitigation in end-pumped solid-state lasers," J. Phys. D **34**(16), 2381–2395 (2001).
7. M. Tsunekane, N. Taguchi, and H. Inaba, "Improvement of thermal effects in a diode-end-pumped, composite Tm:YAG rod with undoped ends," Appl. Opt. **38**(9), 1788–1791 (1999).
8. Y. T. Chang, Y. P. Huang, K. W. Su, and Y. F. Chen, "Comparison of thermal lensing effects between single-end and double-end diffusion-bonded Nd:YVO_4 crystals for $^4F_{3/2}\rightarrow{}^4I_{11/2}$ and $^4F_{3/2}\rightarrow{}^4I_{13/2}$ transitions," Opt. Express **16**(25), 21155–21160 (2008).
9. I. I. Kuznetsov, I. B. Mukhin, D. E. Silin, A. G. Vyatkin, O. L. Vadimova, and O. V. Palashov, "Thermal effects in end-pumped Yb:YAG thin-disk and Yb:YAG/YAG composite active element," IEEE J. Quantum Electron. **50**(3), 133–140 (2014).
10. J. Song, A. Liu, K. Okino, and K. Ueda, "Control of the thermal lensing effect with different pump light distributions," Appl. Opt. **36**(30), 8051–8055 (1997).
11. M. Frede, R. Wilhelm, M. Brendel, C. Fallnich, F. Seifert, B. Willke, and K. Danzmann, "High power fundamental mode Nd:YAG laser with efficient birefringence compensation," Opt. Express **12**(15), 3581–3589 (2004).

#274931 http://dx.doi.org/10.1364/OE.24.026024
Journal © 2016 Received 31 Aug 2016; revised 14 Oct 2016; accepted 23 Oct 2016; published 1 Nov 2016

Optics EXPRESS

12. M. S. Roth, E. W. Wyss, T. Graf, and H. P. Weber, "End-pumped Nd:YAG laser with self-adaptive compensation of the thermal lens," IEEE J. Quantum Electron. **40**(12), 1700–1703 (2004).
13. H. Chen, Q. Liu, X. Yan, and M. Gong, "High power Q-switched TEM_{00} Nd:YVO_4 laser with self-adaptive compensation of thermal lensing effect," Laser Phys. **20**(7), 1594–1597 (2010).
14. Y. F. Chen, "Pump-to-mode size ratio dependence of thermal loading in diode-end-pumped solid-state lasers," J. Opt. Soc. Am. B **17**(11), 1835–1840 (2000).
15. A. Giesen, H. Hügel, A. Voss, K. Wittig, U. Brauch, and H. Opower, "Scalable concept for diode-pumped high-power solid-state lasers," Appl. Phys. B **58**(5), 365–372 (1994).
16. B. J. Garrec, G. J. Razé, P. Y. Thro, and M. Gilbert, "High-average-power diode-array-pumped frequency-doubled YAG laser," Opt. Lett. **21**(24), 1990–1992 (1996).
17. S. H. Cho, B. E. Bouma, E. P. Ippen, and J. G. Fujimoto, "Low-repetition-rate high-peak-power Kerr-lens mode-locked Ti:Al_2O_3 laser with a multiple-pass cavity," Opt. Lett. **24**(6), 417–419 (1999).
18. W. Koechner, *Solid-State Laser Engineering*, 6th ed. (Springer, 2006).
19. R. B. Chesler and D. Maydan, "Convex-concave resonators for TEM_{00} operation of solid-state ion lasers," J. Appl. Phys. **43**(5), 2254–2257 (1972).
20. W. A. Clarkson, R. Koch, and D. C. Hanna, "Room-temperature diode-bar-pumped Nd:YAG laser at 946 nm," Opt. Lett. **21**(10), 737–739 (1996).
21. J. J. Kasinski, W. Hughes, D. DiBiase, P. Bournes, and R. Burnham, "One Joule output from a diode-array-pumped Nd:YAG laser with side-pumped rod geometry," IEEE J. Quantum Electron. **28**(4), 977–985 (1992).
22. C. Y. Cho, Y. P. Huang, Y. J. Huang, Y. C. Chen, K. W. Su, and Y. F. Chen, "Compact high-pulse-energy passively Q-switched Nd:YLF laser with an ultra-low-magnification unstable resonator: application for efficient optical parametric oscillator," Opt. Express **21**(2), 1489–1495 (2013).
23. G. Q. Xie, D. Y. Tang, L. M. Zhao, L. J. Qian, and K. Ueda, "High-power self-mode-locked Yb:Y_2O_3 ceramic laser," Opt. Lett. **32**(18), 2741–2743 (2007).
24. H. C. Liang, R. C. Chen, Y. J. Huang, K. W. Su, and Y. F. Chen, "Compact efficient multi-GHz Kerr-lens mode-locked diode-pumped Nd:YVO_4 laser," Opt. Express **16**(25), 21149–21154 (2008).
25. F. Krausz, T. Brabec, and C. Spielmann, "Self-starting passive mode locking," Opt. Lett. **16**(4), 235–237 (1991).
26. F. Bretenaker and N. Treps, *Laser: 50 Years of Discoveries* (World Scientific, 2015).
27. E. Hechit, *Optics*, 4th ed. (Addison-Wesley, 1998), Chap. 5.
28. N. Hodgson and H. Weber, *Laser Resonators and Beam Propagation*, 2nd ed. (Springer, 2005), Chaps. 8 and 12.
29. A. Agnesi, E. Piccinini, and G. C. Reali, "Influence of thermal effects in Kerr-lens mode-locked femtosecond Cr^{4+}:forsterite lasers," Opt. Commun. **135**(1–3), 77–82 (1997).
30. A. Agnesi, C. Pennacchio, G. C. Reali, and V. Kubecek, "High-power diode-pumped picosecond $Nd(^{3+})$:$YVO(_4)$ laser," Opt. Lett. **22**(21), 1645–1647 (1997).
31. P. Li, Q. P. Wang, X. Y. Zhang, J. Lian, J. Chang, Z. J. Liu, S. Z. Fan, and X. H. Chen, "Compact and efficient Kerr-lens mode-locked diode-pumped actively Q-switched YVO_4-Nd:YVO_4 laser," Opt. Commun. **283**(24), 5139–5144 (2010).
32. H. C. Liang, Y. J. Huang, W. C. Huang, K. W. Su, and Y. F. Chen, "High-power, diode-end-pumped, multigigahertz self-mode-locked Nd:YVO_4 laser at 1342 nm," Opt. Lett. **35**(1), 4–6 (2010).
33. Y. F. Chen, H. C. Liang, J. C. Tung, K. W. Su, Y. Y. Zhang, H. J. Zhang, H. H. Yu, and J. Y. Wang, "Spontaneous subpicosecond pulse formation with pulse repetition rate of 80 GHz in a diode-pumped Nd:$SrGdGa_3O_7$ disordered crystal laser," Opt. Lett. **37**(4), 461–463 (2012).
34. H. C. Liang, T. W. Wu, J. C. Tung, C. H. Tsou, K. F. Huang, and Y. F. Chen, "Total self-mode locking of multi-pass geometric modes in diode-pumped Nd:YVO_4 lasers," Laser Phys. Lett. **10**(10), 105804 (2013).
35. Y. Zhang, H. Yu, H. Zhang, A. Di Lieto, M. Tonelli, and J. Wang, "Laser-diode pumped self-mode-locked praseodymium visible lasers with multi-gigahertz repetition rate," Opt. Lett. **41**(12), 2692–2695 (2016).
36. Y. Zhang, H. Yu, H. Zhang, X. Xu, J. Xu, and J. Wang, "Self-mode-locked Laguerre-Gaussian beam with staged topological charge by thermal-optical field coupling," Opt. Express **24**(5), 5514–5522 (2016).
37. C. L. Sung, H. P. Cheng, C. Y. Lee, C. Y. Cho, H. C. Liang, and Y. F. Chen, "Generation of orthogonally polarized self-mode-locked Nd:YAG lasers with tunable beat frequencies from the thermally induced birefringence," Opt. Lett. **41**(8), 1781–1784 (2016).
38. H. Liu, J. Nees, and G. Mourou, "Diode-pumped Kerr-lens mode-locked Yb:$KY(WO_4)_2$ laser," Opt. Lett. **26**(21), 1723–1725 (2001).
39. M. T. Chang, H. C. Liang, K. W. Su, and Y. F. Chen, "Dual-comb self-mode-locked monolithic Yb:KGW laser with orthogonal polarizations," Opt. Express **23**(8), 10111–10116 (2015).
40. Y. F. Chen, M. T. Chang, W. Z. Zhuang, K. W. Su, K. F. Huang, and H. C. Liang, "Generation of sub-terahertz repetition rates from a monolithic self-mode-locked laser coupled with an external Fabry-Perot cavity," Laser Photonics Rev. **9**(1), 91–97 (2015).
41. Y. F. Chen, Y. J. Huang, P. Y. Chiang, Y. C. Lin, and H. C. Liang, "Controlling number of lasing modes for designing short-cavity self-mode-locked Nd-doped vanadate lasers," Appl. Phys. B **103**(4), 841–846 (2011).

1. Introduction

Diode-end-pumped solid-state lasers have been widely adopted because of its high efficiency, compactness, reliability, and good beam quality [1]. However, the small volume of the end-

Optics EXPRESS

pumping profile usually causes a serious thermal lensing effect which significantly influences the laser stability, oscillation mode size, output beam quality, and the maximum achievable average power [2–6]. In order to achieve power scaling for end-pumped lasers, several approaches such as using the composite crystal as the gain medium [7–9], controlling the pump distribution [10,11], and employing the self-adaptive compensation [12,13] have been proposed to treat the thermal lensing effect. Although these methods can improve the laser performance under the thermal lensing to a certain extent, the cavity length for most configurations is inevitably limited by the thermally induced instability under a high pump power [14]. For a stable operation under thermal lensing with a long cavity length, the resonator is frequently designed to have V-shaped or even more complicated configuration [15–17] which makes cavity alignment very difficult. Consequently, a compact and reliable design of linear resonators with a great compensation ability for thermal lensing in flexible cavity lengths is highly desirable for mode-locked or Q-switched operations with widely tunable pulse repetition rates and pulse widths [18].

It has been known that using a convex mirror as the cavity front mirror can effectively compensate the thermal lensing effect [19, 20]. Nevertheless, most applications of the convex-concave resonator focus on the unstable operation to enlarge the fundamental mode volume [21, 22]. So far there are few discussions about the performance of a convex-concave stable resonator under strong thermal lensing effect. In this work, the convex-concave resonator is thoroughly studied to design a linear cavity with excellent compensation ability to thermal lensing in stable operation. It is intriguingly found that the critical thermal power of the proposed resonator is solely determined by the radius of curvature of the convex front mirror but not restricted by the cavity length. More importantly, the cavity analysis shows that the oscillation mode size under stable operation remains nearly unchanged with not only the increasing thermal power but also the variation of cavity length. These superior advantages of the convex-concave resonator enable us to easily achieve power scaling for continuous-wave lasers with flexible cavity lengths. On the other hand, since the mode-matching condition between the pump and cavity modes can be easily controlled to be almost the same, we further apply the proposed cavity to explore the influence of cavity length on self-mode-locked (SML) operation [23, 24]. As proposed by Krausz *et al* [25] that the cavity length plays an important role for the self-starting mode locking in free-running lasers, the multi-pulse mode-locked state corresponding to optical spectrum with multiple groups of lasing modes is observed when the cavity length increases. Finally, we develop a theoretical model to reconstruct the experimental results of the SML operation to deduce a simple relationship between the group number of lasing modes and the cavity length. The current study of the convex-concave resonator sheds light on its applicability to achieve mode-locked or Q-switched lasers with flexibly tunable pulse repetition rates and pulse widths for various applications [26].

2. Cavity configuration and analysis

The configuration of the convex-concave resonator is schematically depicted in Fig. 1. The input front mirror (FM) is a plano-convex mirror with the radius of curvature R_1 and the output coupler (OC) is a concave-plano mirror with the radius of curvature R_2. Note that R_1 is negative and R_2 is positive under the sign convention for general ABCD law in optics. It is worth to mention that the convex FM cannot only be used to compensate the thermal lens of the gain crystal but also simultaneously serve as a reimaging lens to make the whole system more compact. According to the thin lens formula [27], the effective focal length of the plano-convex mirror with the refractive index to be 1.5 can be estimated to be $f_r \approx 2|R_1|$. Therefore, the distance from the convex FM to the principle plane of the gain medium is set to be $d_1 = 2|R_1|$ for effective pumping. By using the condition of $0 \le g_1 g_2 \le 1$ in cavity theory, where $g_i = 1-(d_1 + d_2)/R_i$ [28], the stable region for the cavity length L_{cav} of convex-concave resonator under the cold-cavity assumption can be determined to range from $L_{cav} = R_2-|R_1|$ to

Optics EXPRESS

$L_{cav} = R_2$ provided $|R_2|>|R_1|$. Here d_2 is the distance from the principal plane of gain medium to the concave OC.

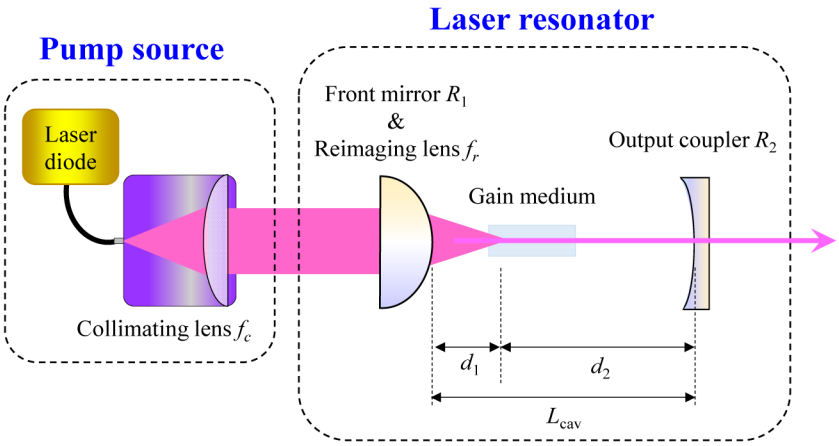

Fig. 1. Experimental configuration for the end-pumped laser with the convex-concave resonator.

To analyze the stable criterion for convex-concave resonator influenced by the internal thermal lens, the equivalent g^*-parameter given by [28]

$$g_i^* = g_i - D d_j \left(1 - \frac{d_i}{R_i}\right), \quad i, j = 1,2 \ \& \ i \neq j \tag{1}$$

is employed, where D is the refractive power of the thermal lens that is proportional to the pump power [3]. Substituting Eq. (1) into the condition of $g_1^* g_2^* = 0$, a quadratic equation given by

$$\left(d_1 - \frac{d_1^2}{R_1}\right)\left(d_2 - \frac{d_2^2}{R_2}\right)D^2 - \left[g_1\left(d_1 - \frac{d_1 d_2}{R_2}\right) + g_2\left(d_2 - \frac{d_1 d_2}{R_1}\right)\right]D + g_1 g_2 = 0 \tag{2}$$

can be derived to determine the critical refractive power D_{crit} for stable operation. Note that here we only consider $g_1^* g_2^* = 0$ because it is the more critical condition to determine the stability of convex-concave resonator under the thermal lensing effect. After simple algebra, the roots of Eq. (2) can be solved as

$$D_i = \frac{R_j - (d_1 + d_2)}{d_i R_j - d_1 d_2}, \quad i, j = 1,2 \ \& \ i \neq j. \tag{3}$$

Considering the thermal lens to be a thin lens which gives $d_1 + d_2 = L_{cav}$ and setting the cavity length $L_{cav} = R_2 - |R_1|$, the smaller solution given by Eq. (3) can lead to

$$D_{crit} = \frac{1}{6|R_1|}. \tag{4}$$

This intriguing result indicates that a wide stable range of refractive power can be easily achieved by adequately decreasing $|R_1|$ of the convex FM.

Next we analyze the dependence of the oscillation mode size upon the refractive power D to examine the compensation ability against the thermal lensing for the convex-concave resonator. Using the g*-parameters and the effective cavity length given by $L^* = d_1 + d_2 -$

Optics EXPRESS

Dd_1d_2, the effective mode size ω_c at the principal plane of gain medium for an optical resonator with an inner thermal lens can be expressed as

$$\omega_c = \sqrt{\frac{\lambda L^*}{\pi}\sqrt{\frac{g_2^*}{g_1^*(1-g_1^*g_2^*)}}\left[\left(1-\frac{d_1}{R_1}\right)^2+\left(\frac{d_1}{L^*}\right)^2\frac{g_1^*(1-g_1^*g_2^*)}{g_2^*}\right]}, \tag{5}$$

where λ is the emission wavelength of the laser. Figure 2 shows the numerical calculations of ω_c as a function of D with different R_1 and R_2 for the convex-concave resonator. Note that the stability zone of operation for the proposed cavity belongs to the zone-I type that does not exhibit a critical divergence of alignment sensitivity. Once the convex-concave resonator has been aligned, a good TEM_{00} mode operation with an excellent beam quality can be achieved even at a high pump level as seen in later discussions. From Fig. 2 it can be seen that the cavity mode size ω_c is positively correlated to the value of $|R_1|$ but nearly independent of R_2 for all these cases. In other words, ω_c of the convex-concave resonator can be controlled almost the same with flexible cavity lengths once $|R_1|$ is fixed. More importantly, it can be also found that ω_c remains almost unchanged with the refractive power in the stable region $D = 0.2D_{crit}$~$0.85D_{crit}$. These numerical results reveal that the proposed resonator has excellent stability even under strong thermal lensing effect. To obtain a more transparent expression for ω_c in terms of R_1 and R_2 in stable operation, we set $D = 1/(12|R_1|)$ in Eq. (1) and use Eq. (5) for further simplification. After some algebra, the dependence of ω_c on R_1 and R_2 can be evaluated as

$$\omega_c = \sqrt{\frac{6\lambda|R_1|}{\pi}\cdot\left(\sqrt{\frac{5R_2-3|R_1|}{3R_2+3|R_1|}}+\sqrt{\frac{3R_2+3|R_1|}{5R_2-3|R_1|}}\right)}. \tag{6}$$

Equation (6) clearly reveals that $\omega_c \propto (|R_1|)^{1/2}$ as long as $|R_2|$ is fairly larger than $|R_1|$. As a consequence, the good matching between the pump and cavity modes can be easily achieved in the proposed resonator with a very wide range of cavity length.

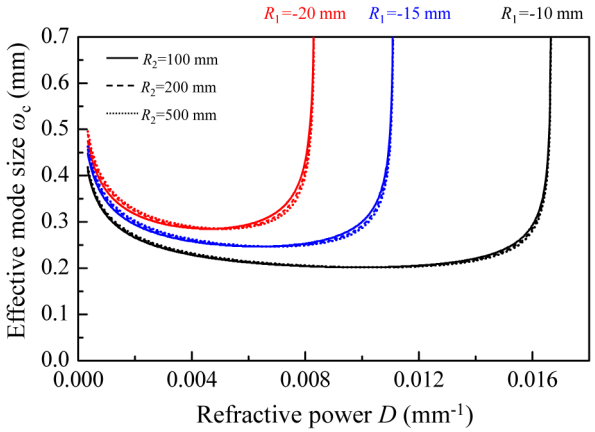

Fig. 2. Numerical calculations of effective mode size ω_c as a function of the refractive power D with different R_1 and R_2 for the convex-concave resonator.

3. Experimental confirmation

For experimentally verifying the particular characteristics predicted by the cavity analysis, the convex-concave resonator is utilized to demonstrate a continuous-wave (CW) laser. To highlight the features of the proposed resonator and to estimate the typical level of refractive power for common solid-state lasers, we studied the CW performance of a conventional

Optics EXPRESS

concave-plano cavity first as the experimental counterpart. The pump source was a 29-W 808-nm fiber-coupled laser diode with a 600-μm core diameter and a 0.2 numerical aperture. The gain medium was a 0.2 at. % a-cut Nd:YVO_4 crystal with dimensions of 3 × 3 × 10 mm^3. The laser crystal was wrapped with indium foil and mounted in a water-cooled copper heat sink at 16°C. The pump beam was reimaged into the gain medium by a coupling lens set with a 38-mm effective focal length and a unity magnification. The pump spot size ω_p on the gain medium is about 300 μm. The FM was a 900-mm radius-of-curvature concave mirror coated with antireflection (AR) at 808 nm on the entrance face and high-reflection (HR) at 1064 nm on the second surface. A plane mirror with 5% transmission at 1064 nm was used as the OC. Considering the typical case of an end-pumping concave-plano cavity, the gain medium was placed fairly close to the FM, i.e. $d_1 \to 0$. Figure 3(a) shows the performance of average output power versus input pump power for the concave-plano CW laser measured at L_{cav} = 80, 180, 280, and 480 mm. It can be found that the average output power displays an obvious descent with the increasing pump power for the cases with longer cavity lengths. Due to the fact that the critical refractive power $D_{crit} \approx 1/L_{cav}$ for the concave-plano cavity with $d_1 \to 0$ [14], the longer the cavity length of concave-plano cavity is the smaller the stable range it has. From the experimental results, the dependence of refractive power for the thermal lens upon the pump power is further estimated as shown by the upper abscissa of Fig. 3.

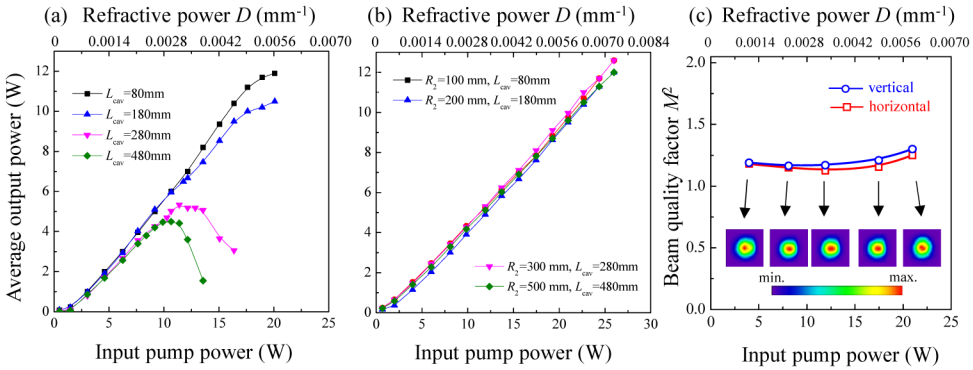

Fig. 3. CW performances of average output power versus input pump power for the cases of (a) concave-plano and (b) convex-concave resonators with L_{cav} = 80, 180, 280, and 480 mm. (c) The beam quality factor and laser transverse patterns versus input pump power for the convex-concave resonator with L_{cav} = 80 mm.

To compare the CW performance of the proposed convex-concave cavity with that of the conventional concave-plano cavity, we changed the FM to be a convex mirror with a radius-of-curvature R_1 and replaced the plane OC by a concave OC with a radius-of-curvature R_2 as shown in Fig. 1. It has been experimentally confirmed that all the performances for the configurations with different R_1 and R_2 discussed in Sec. 2 are consistent with the theoretical analyses. But for a concise presentation here, we only choose the case of R_1 = –20 mm as a paradigm. To be consistent with previous analysis, we set $L_{cav} = R_2 - |R_1|$ in the experiment. Therefore, the cavity length can be adjusted the same as the cases for concave-plano cavity by choosing R_2 to be 100, 200, 300, and 500 mm. The focal length of the collimating lens was set to be f_c = 38 mm for remaining similar pumping condition. Figure 3(b) displays the average output power versus the input pump power for the cases of convex-concave resonator with different L_{cav}. It can be clearly seen that the output power can be scaled up beyond 12 W without any trend of thermally induced saturation even for the case with L_{cav} = 480 mm. Besides, the slope efficiency can be easily maintained higher than 50% for all these cases. Furthermore, it is confirmed that the laser beam quality can remains quite good for all these cases with different L_{cav} even at a high pump level. Figure 3(c) shows the beam quality M^2 factor versus the pump power for the convex-concave resonator with L_{cav} = 80 mm as a

Optics EXPRESS

reference. The corresponding laser patterns are shown as the insets of Fig. 3(c). It can be observed that the overall values of M^2 can be maintained to be below 1.3 for all the cases even when the pump power has exceeded 20 W. The remarkable output performance validates that the proposed convex-concave resonator definitely has quite excellent stability with flexible cavity lengths even under strong thermal lensing effect. This superior advantage of the proposed resonator paves the way for achieving mode-locked or Q-switched lasers with widely tunable pulse repetition rates and pulse widths for various applications [26].

4. Application: exploring influence of cavity length on the SML operation

The self-mode-locked (SML) phenomenon is an intriguing mean to achieve the mode-locking operation in laser systems without any use of the saturable absorber [23, 24]. The fundamental mechanism of SML is closely related to the Kerr-lens mode locking which exploits the Kerr nonlinearity of the gain medium itself and the soft aperture formed by the end-pumping profile [29–31]. In the early stage of diode-pumped solid-state lasers, Krausz *et al* [25] have derived a simple criterion to analyze the self-starting threshold of the passive mode locking from mode beating fluctuations in a free-running laser. This criterion indicates that a decrease in the cavity round-trip time (so as the cavity length) can significantly reduce the intensity needed for self-starting mode locking at a fixed nonlinearity. Even though the importance of controlling the cavity length to achieve SML operation has been extensively confirmed in the diode-end-pumped solid-state lasers [32–39], a thorough investigation about the influence of increasing cavity length on the temporal behavior of SML phenomenon is seldom reported so far. Since the proposed convex-concave resonator has been proven to not only display fairly well stability under thermal lensing effect but also preserve a good spatial matching between the pump and lasing modes in a wide range of cavity length, it is suitably to be applied to explore the exclusive influence of cavity length on the SML phenomenon. Note that under the assumption that both the pump and laser beams are Gaussian, the overlap efficiency given by $S = (\omega_c^2(\omega_c^2 + 2\omega_p^2))/(\omega_c^2 + \omega_p^2)^2$ [5] can be evaluated to be in the range from about 75% to 85% in the operation region of pump power for the convex-concave resonator.

At first we measured the optical spectra of the convex-concave resonator in SML operations with different cavity lengths by a Michelson-interferometer-type optical spectrum analyzer (Advantest Q8347) with the resolution of 0.003 nm. The experimental conditions were set to be the same as the cases in Sec. III except for the cavity length was slightly adjusted for good SML operation. Figures 4(a)-4(c) show the optical spectra of SML operation in the convex-concave resonator under the input pump power P_{in} = 12 W with L_{cav} = 90, 190, and 290 mm, respectively. It can be clearly found that the spectrum for the case of L_{cav} = 90 mm displays a single-group behavior of lasing longitudinal modes, whereas the lasing modes split into two and three main groups for the cases of L_{cav} = 190 and 290 mm, respectively. Note that even though the mode spacing $\Delta\lambda = (\lambda_c^2/2L_{opt})$ is too small to resolve all lasing longitudinal modes in these cases, the envelopes of the spectra can still be measured to unambiguously reflect the grouping phenomena for the increasing cavity length. Here λ_c is the central wavelength of the laser and L_{opt} is the effective optical length given by $L_{opt} = L_{cav} + (n_r\text{-}1)\, L_g$, where n_r is the refractive index and L_g is the length of the gain crystal.

Optics EXPRESS

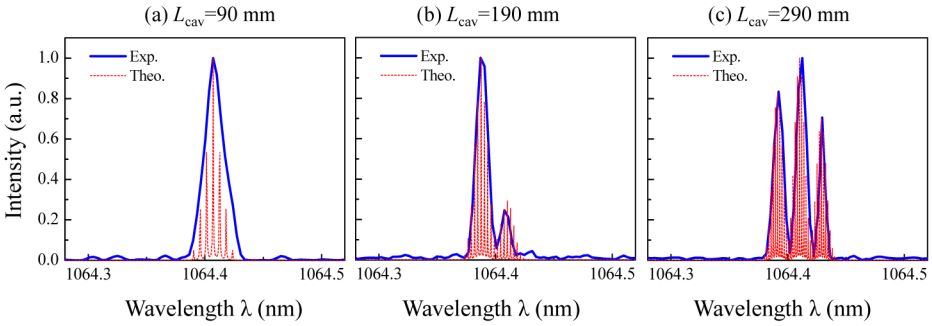

Fig. 4. The measured (blue solid lines) and reconstructed (red dashed lines) optical spectra of SML operation in the convex-concave resonator under an input pump power P_{in} = 12 W with L_{cav} to be (a) 90, (b) 190, and (c) 290 mm.

The temporal traces of the SML operation were detected by a high-speed InGaAs photodetector (Electro-Optics Technology Inc. ET-3500 with rising time 35 ps) and the output signals were connected to a digital oscilloscope (Agilent DSO 80000) with 12 GHz electrical bandwidth and a sampling interval of 25 ps. The upper row of Figs. 5(a)-5(c) display the temporal traces of mode-locked pulse trains with the time span of 10 ns corresponded to the optical spectra shown in Figs. 4(a)-4(c), respectively. For the case of L_{cav} = 90 mm, the pulse train exhibit a clear single-pulse mode-locking behavior that is consistent with the single-group longitudinal modes. On the other hand, due to the fact that the lasing longitudinal modes have split into multiple groups in the spectra, the temporal traces for the cases of L_{cav} = 190 and 290 mm present multi-pulse mode-locked pulse trains with some background noise. Figures 6(a)-6(c) show the long-term temporal behavior for the single-pulse and multi-pulse mode locking in the time span of 5 μs with L_{cav} = 90, 190, and 290 mm, respectively. It can be clearly seen that the oscilloscope traces exhibit quite good amplitude stability no matter for the case of single-pulse mode locking or for the case of multi-pulse mode locking. These experimental results confirm that the matching condition between pump and lasing modes for the fundamental mode operation can be easily maintained in a wide range of cavity length for the proposed convex-concave resonator.

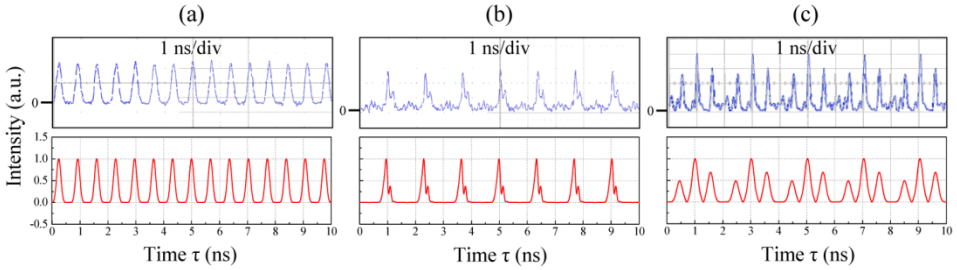

Fig. 5. The measured (upper row) and reconstructed (lower row) mode-locked pulse trains corresponding to optical spectra shown in Figs. 4(a)-4(c) with a time span of 10 ns.

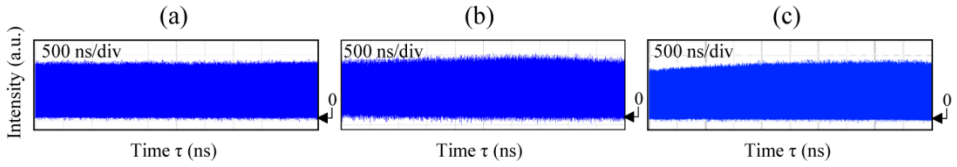

Fig. 6. The long-term behavior of mode-locked pulse trains in the time span of 5 μs for the cases of L_{cav} to be (a) 90, (b) 190, and (c) 290 mm, respectively.

Optics EXPRESS

To further demonstrate that the multi-pulse mode locking can be perfectly explained by the grouping of lasing longitudinal modes, we develop a theoretical model for reconstruction of the experimental spectra and the corresponding temporal states. The spectral domain in the wavelength representation for the m^{th} group consisting of $2M_0 + 1$ longitudinal modes with a constant relative phase ϕ_m can be expressed as [40]

$$\varphi_m(\lambda) = \sum_{n=-M_0}^{M_0} C_{n+M_0}^{2M_0} e^{in\phi_m} \delta(\lambda - \lambda_m - n\cdot\Delta\lambda), \tag{7}$$

where λ_m is the central wavelength of m^{th} group and $\Delta\lambda$ is the longitudinal mode spacing. Note that the weighting coefficient for each mode is assumed to follow a binomial distribution to obtain a concise expression for the temporal state later and to agree with the experimental spectra. By using Eq. (7) the overall profile of the spectral domain in λ-representation for the case with totally M_1 groups of longitudinal modes can be written as

$$\Phi(\lambda) = \sum_{m=1}^{M_1} A_m \varphi_m(\lambda), \tag{8}$$

where A_m is the relative amplitude of the m^{th} group. The optical spectrum can therefore be given by $|\Phi(\lambda)|$ ideally. To manifest the experimental spectrum in a realistic way, the Lorentzian function is used to express the δ-function in Eq. (7). The resultant optical spectrum is then given by

$$I(\lambda) = \left| \frac{1}{\pi} \sum_{m=1}^{M_1} \sum_{n=-M_0}^{M_0} A_m C_{n+M_0}^{2M_0} e^{in\phi_m} \frac{\Gamma\Delta\lambda^2}{(\lambda - \lambda_m - n\cdot\Delta\lambda)^2 + (\Gamma\cdot\Delta\lambda)^2} \right|, \tag{9}$$

where Γ is the effective linewidth of the cavity mode. Note that the central wavelength of the m^{th} group can be written as $\lambda_m = \lambda_1 + N(m\text{-}1)\cdot\Delta\lambda$ provided that there are N spacing between the central longitudinal modes of each group.

The wave function in temporal domain corresponding to the spectrum of lasing longitudinal modes can be directly given by the Fourier transform of $\Phi(\lambda)$ as

$$\Psi(t) = \frac{1}{2^{2M_0}} \sum_{m=1}^{M_1} \sum_{n=-M_0}^{M_0} A_m C_{n+M_0}^{2M_0} e^{i\omega_m t} e^{in(\Delta\omega t + \phi_m)} = \sum_{m=1}^{M_1} A_m e^{i\omega_m t} \left\{ \cos\left[(\Delta\omega\cdot t + \phi_m)/2 \right] \right\}^{2M_0}, \tag{10}$$

where $\omega_m = 2\pi c/\lambda_m$ is the angular frequency of the central mode for the m^{th} group, $\Delta\omega = \pi c/L_{opt}$, and c is the light speed in vacuum. Here we have used the equivalence of $\sum_{k=0}^{2M} (C_k^{2M} x^k) /2^{2M} = (1 + x)^{2M}/2^{2M}$ for obtaining a concise expression. The factor of $1/2^{2M0}$ is included for normalizing the superposition of single-group longitudinal modes. The term $\{\cos[(\Delta\omega\cdot t + \phi_m)/2]\}^{2M0}$ in Eq. (10) indicates that the single-group mode-locked state exhibits a pulse train with the peaks at $t = Mt_r - (\phi_m\cdot t_r)/2\pi$, where $M = 0, \pm 1, \pm 2, \ldots$ and $t_r = 2L_{opt}/c$ is the cavity round-trip time. Hence the initial position of the pulse train can be straightforwardly shifted by varying ϕ_m. On the other hand, the number of longitudinal modes M_0 in each group directly determines the width of the mode-locked pulse based on the property of the cosine function. As a result, the overall structures of the oscilloscope traces can be reconstructed by suitably controlling the parameters of M_0 and ϕ_m.

The lower rows of Figs. 5(a)-5(c) illustrate the numerical results of $|\Psi(t)|^2$ with the parameters shown as follows: (a) $M_0 = 3$, $M_1 = 1$, $\phi_1 = 0$, $A_1 = 1$; (b) $M_0 = 7$, $M_1 = 2$, $N = 8$, $\phi_1 = 0$, $\phi_2 = 0.25\pi$, $A_1 = 1$, $A_2 = 0.3$; (c) $M_0 = 10$, $M_1 = 3$, $N = 10$, $\phi_1 = -0.55\pi$, $\phi_2 = 0$, $\phi_3 = 0.55\pi$, $A_1 = 0.83$, $A_2 = 1$, $A_3 = 0.7$. Note that M_0, M_1, N, and A_m are directly determined by the characteristics of experimental spectra while ϕ_m is chosen to fit the detailed structures of

Optics EXPRESS

mode-locked pulses of the oscilloscope traces. The wavelength of the central mode for the first group was set to be $\lambda_1 \approx 1064.4$ nm in these cases. To give thorough comparisons to the experimental results, the reconstructed spectra $I(\lambda)$ calculated by Eq. (9) corresponding to the temporal traces in Figs. 5(a)-5(c) are also shown by the red dashed lines in Figs. 4(a)-(c). It can be clearly seen that the temporal traces given by the reconstructed spectra can perfectly describe all the experimental data. The good agreement between the experimental observation and the theoretical reconstruction verifies that the grouping behavior of lasing modes can explain the origin of multi-pulse mode locking very well.

Finally, we deduce a simple relationship between the group number of lasing modes and the cavity length from the experimental results of SML operation in the convex-concave resonator as shown in Fig. 7. It can be obviously seen that the group number M_1 is approximately proportional to the cavity length L_{cav} as L_{cav} >100 mm. For the case with fairly long cavity length, the large number of groups of lasing modes will lead the temporal behavior to present very complicated multi-pulse mode locking in the SML operation as seen in Fig. 7. It is believed that the grouping phenomenon of lasing longitudinal modes under a long cavity length is related to the spatial hole burning effect for efficiently depleting the residual gain in the gain medium [41]. Unlike typical Kerr-lens mode-locked Ti:Sapphire lasers with broader and smoother gain bandwidth which can sustain a consecutive longitudinal-mode lasing in a single-group spectrum [17], lasers with narrower and sharper gain such as the Nd-doped crystal lasers may prefer generating longitudinal modes in different groups to consume the spatial gain more effectively when the mode spacing is fairly small under a similar spatial hole burning condition [41]. Nevertheless, the complete theory to analyze the dependence of group number upon the cavity length and the special gain dig phenomenon is beyond the scope of this work and must be left for future investigations.

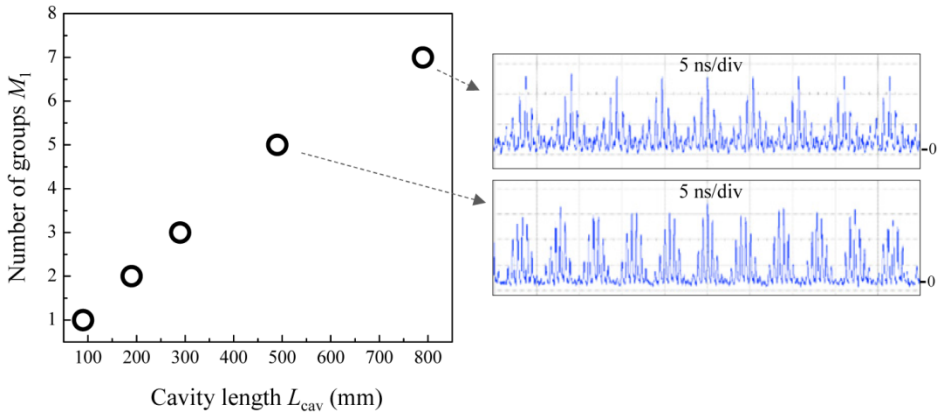

Fig. 7. The relationship between the group number of lasing modes and the cavity length for the SML operations in the convex-concave resonator.

5. Summary

In conclusion, we have thoroughly studied the performances of convex-concave resonator under the influence of thermal lensing effect. The theoretical analysis reveals that the proposed resonator has an excellent compensation ability against the thermal lensing to make the cavity mode size remain nearly unchanged with the refractive power in a wide range of cavity length. Consequently, by exploiting the advantage of the proposed resonator we have achieved the power scaling of CW lasers with flexible cavity lengths. Moreover, since the good matching condition between the pump and cavity modes can be easily sustained in the convex-concave resonator, it has been further applied to explore the influence of cavity length on SML operation. It has been found that the lasing longitudinal modes will split into multiple groups to lead the temporal states to present the multi-pulse mode-locking behavior when the

Optics EXPRESS

cavity length increases. With the perfect reconstruction for the optical spectra and the mode-locked pulse trains by a theoretical model, we have deduced a simple relationship between the group number of longitudinal modes and the cavity length. The current findings shed light on using the convex-concave resonator to design mode-locked or Q-switched lasers with flexible pulse repetition rates and pulse widths for various applications.

Funding

Ministry of Science and Technology of Taiwan (Contract No. MOST-105-2628-M-009-004).